

Rapid Intensification of a Sheared Tropical Storm

JOHN MOLINARI AND DAVID VOLLARO

*Department of Atmospheric and Environmental Sciences, University at Albany,
State University of New York, Albany, New York*

(Manuscript received 10 February 2010, in final form 28 April 2010)

ABSTRACT

A weak tropical storm (Gabrielle in 2001) experienced a 22-hPa pressure fall in less than 3 h in the presence of 13 m s^{-1} ambient vertical wind shear. A convective cell developed downshear left of the center and moved cyclonically and inward to the 17-km radius during the period of rapid intensification. This cell had one of the most intense 85-GHz scattering signatures ever observed by the Tropical Rainfall Measuring Mission (TRMM). The cell developed at the downwind end of a band in the storm core. Maximum vorticity in the cell exceeded $2.5 \times 10^{-2} \text{ s}^{-1}$. The cell structure broadly resembled that of a vortical hot tower rather than a supercell.

At the time of minimum central pressure, the storm consisted of a strong vortex adjacent to the cell with a radius of maximum winds of about 10 km that exhibited almost no tilt in the vertical. This was surrounded by a broader vortex that tilted approximately left of the ambient shear vector, in a similar direction as the broad precipitation shield. This structure is consistent with the recent results of Riemer et al.

The rapid deepening of the storm is attributed to the cell growth within a region of high efficiency of latent heating following the theories of Nolan and Vigh and Schubert. This view is supported by a rapid growth of wind speed and vorticity in the storm core during the 1-h lifetime of the cell, and by the creation of a narrow 7°C spike in 700-hPa temperature adjacent to the cell and coincident with the lowest pressure. The cell is not seen as the *cause* of rapid intensification. Rather, it is part of a multiscale process: (i) development of a new circulation center within the downshear precipitation shield, (ii) continued ambient shear creating a favored region for cell formation just downshear of the new center, and (iii) the development of the intense cell that enhanced diabatic heating close to the center in a region of high efficiency of kinetic energy production. This sheared, asymmetric rapid intensification of Tropical Storm Gabrielle is contrasted with the nearly symmetric composite given by Kaplan and DeMaria.

1. Introduction

Kaplan and DeMaria (2003, 2010) described the conditions most likely to accompany rapid intensification of tropical cyclones. The presence of small ambient vertical wind shear and a symmetric distribution of deep convective clouds around the center were among the strongest of their criteria. Occasionally, however, rapid intensification occurs in storms with large ambient vertical wind shear and a strongly asymmetric structure. The nature of this asymmetric rapid intensification of sheared storms has only begun to be addressed in the literature.

Sheared tropical cyclones contain stronger convergence and upward motion downshear and especially

downshear left (Black et al. 2002; Reasor et al. 2009; Braun et al. 2006). They also contain larger CAPE, helicity, and local vertical wind shear downshear (Molinari and Vollaro 2008, 2010). All of these factors support the observed preference for convection downshear (e.g., Corbosiero and Molinari 2002; Chen et al. 2006), and the potential for severe convective cells in the same region (Molinari and Vollaro 2010).

One common behavior in sheared tropical cyclones is the growth of cells downshear in the storm core and their subsequent dissipation upshear (Heymssfield et al. 2001; Black et al. 2002). The rapid intensification of Hurricane Guillermo (1997) in the presence of 8 m s^{-1} ambient vertical shear has been studied by Eastin et al. (2005), Reasor et al. (2009), and Sitkowski and Barnes (2009). Eastin et al. (2005) found buoyant eyewall updrafts greater than 2 m s^{-1} concentrated downshear-left and left of ambient shear at the 5.5-km level. The source of eyewall buoyancy appeared to be air from within the eye

Corresponding author address: John Molinari, Department of Atmospheric and Environmental Sciences, University at Albany, State University of New York, ES-225, 1400 Washington Ave., Albany, NY 12222.
E-mail: molinari@atmos.albany.edu

that was carried to the eyewall by mesoscale vortices. Reasor et al. (2009) noted that rapid intensification (RI) occurred during the development of clusters of convective cells downshear left associated with mesoscale ascent forced by the ambient shear. Sitkowski and Barnes (2009) showed that a partial eyewall left of the ambient shear repeatedly spiraled into the storm core during the period of rapid deepening.

Although it is a less common event, some storms experience RI even though ambient vertical wind shear is above 10 m s^{-1} . Hurricane Claudette (2003) deepened rapidly in large ambient shear as strong downshear convection reached the storm core (Shelton and Molinari 2009). In the presence of continuing large shear, the storm quickly weakened and was a hurricane for only 6 h. At hurricane strength, extremely dry air upshear created an enormous radial gradient of equivalent potential temperature (6 K km^{-1}) just outside the eyewall. Shelton and Molinari (2009) argued that the dry air resulted from shear-induced subsidence. They further hypothesized that cold downdrafts arising from the mixing of this dry air into the core caused the reversal of deepening. This argument is consistent with the downward flux of low entropy air in simulated storms with large ambient shear found by Riemer et al. (2010).

Tropical storm (TS) Gabrielle (2001), the subject of this study, also experienced a period of RI in the presence of ambient vertical wind shear above 10 m s^{-1} (Molinari et al. 2006). The storm weakened slightly thereafter, and did not reach hurricane strength for more than 2 days.

Hurricane Dennis (2005) experienced RI in the presence of small ambient vertical wind shear. In a simulation of that storm, Rogers (2010) showed two isolated convective cells on either side of the storm core (his Fig. 5d) just prior to the period of RI. These cells contained locally strong vertical velocity above 5 m s^{-1} and were located inside the radius of maximum winds. Rogers (2010) separated convective and stratiform regions. The onset of rapid intensification came about as a result of increased vertical mass flux in the lowest 1.5 km associated with an increase in the areal coverage of convection. Increases in stratiform precipitation occurred only after RI began.

The storms described above exhibit one common attribute and one key difference in behavior. All experienced significant diabatic heating within the radius of maximum winds (RMW) just prior to RI. This can be seen in key figures from each paper: Fig. 5 from Sitkowski and Barnes (2009), Fig. 5 from Shelton and Molinari (2009), Fig. 7 from Molinari et al. (2006), and Fig. 5d from Rogers (2010). Two recent idealized studies in the literature address the importance of the location of heating. Vigh and Schubert (2009), using a balance model, found that heating inside the RMW was much more effective in

strengthening the warm core (and thus intensifying the storm) than heating outside the RMW. Using a linearized primitive equation model, Nolan et al. (2007) defined kinetic energy efficiency (KEE), the relative efficiency of latent heating in generating kinetic energy of the circulation. Nolan (2007) argued that tropical cyclone genesis in his model occurred by a process in which first a mid-level vortex strengthened, producing a large increase in KEE in the storm core. Subsequently any heating that occurred near the center was far more efficient in generating a circulation. Even prior to the growth of the midlevel vortex, maximum KEE occurred from $r = 0$ to $r = 40 \text{ km}$ at elevations from 6–10 km. Based on those results, it will be argued in this paper that any heating in the middle and upper troposphere at small radii should favor deepening, as long as it occurs within the broad radius of maximum wind common in weak storms. This is consistent with the results of Vigh and Schubert (2009) described above.

Although all the storms above experienced diabatic heating within the RMW, they differed in their final intensity. The storms with low or moderate ambient shear (Dennis and Guillermo) became major hurricanes. In contrast, highly sheared storms Claudette and Gabrielle did not reach more than minimal hurricane intensity before weakening. Rapidly intensifying storms in large ambient shear might be limited in intensity by the large shear, as was recently proposed by J. Beven (2009, personal communication, via the Tropical Storms list).

In the previous study of TS Gabrielle (2001), Molinari et al. (2006) described the influence of an approaching upper level trough on the evolution of the storm. The current paper will revisit TS Gabrielle (2001), but will focus on the structure of an intense convective cell and its role in the sheared, asymmetric rapid intensification of the storm.

2. Data sources and calculation methods

The data sources for this study comprise (i) cloud-to-ground lightning locations from the National Lightning Detection Network (NLDN; Cummins et al. 2006; Cummins and Murphy 2009); (ii) aircraft reconnaissance data from the U.S. Air Force, who flew through the center six times between 0000 and 1200 UTC 14 September; (iii) 6-hourly gridded analyses from the European Centre for Medium-Range Weather Forecasts (ECMWF); (iv) Weather Surveillance Radar-1988 Doppler (WSR-88D) radar data from Tampa, Florida; and (v) one overpass from the Tropical Rainfall Measuring Mission (TRMM) suite of instruments. Use of the first three in tropical cyclones has been described in detail by Molinari et al. (2004, 2006). One additional step was taken in processing

the lightning data. Consistent with the findings of Biagi et al. (2007; see Cummins and Murphy 2009), all positive cloud-to-ground flashes with peak current below 10 kA and half the flashes between 10 and 20 kA were removed, because these are likely to represent intracloud flashes.

The thermodynamic fields in the reconnaissance data are subject to sensor wetting errors (Eastin et al. 2002). Based on U.S. Air Force adjustments for supersaturation, such errors are most likely where the temperature is unrealistically low and the air is saturated. (One point near 0848 UTC in Fig. 12 likely contains such an error. This error will not influence the interpretations of the reconnaissance data.)

The Tampa radar was positioned 130–150 km north-east of the center of TS Gabrielle during the times of interest in this study, and almost all of the precipitation was on the same side of the storm as the radar. This distance is close enough for meaningful radar reflectivity and Doppler velocity estimates (e.g., Klazura and Imy 1993). Even after level III processing (Crum and Alberty 1993), a few examples of apparent aliasing and range folding existed. Doppler winds and vorticity from the radar are shown only at the times and locations where no evidence for these problems was present. Stewart and Lyons (1996) describe the use of WSR-88D reflectivity and radial velocity in tropical cyclones.

One significant shortcoming is present in the WSR-88D level III Doppler winds. Apparently in order to aid in display, the data are sorted into bins of constant radial velocity. The vorticity field calculated from this radial velocity is problematic, because it contains meaningful maxima in regions of strong velocity gradients, but also narrow spurious maxima between bins. This problem is bypassed in the current paper by contouring vorticity only at or above $0.5 \times 10^{-2} \text{ s}^{-1}$. This value is larger than any vorticity that arises from the artificial boundaries between the binned data. A limitation of this method is that no true vorticity fields of lesser magnitude can be identified; it isolates intense vorticity maxima only. Doppler winds themselves will also be shown so the reader can see the structure of the wind throughout the storm circulation.

The vorticity from the Doppler winds represents, of course, only one component of the relative vorticity. It is calculated using a cylindrical coordinate centered on the radar:

$$\zeta = -\frac{1}{R} \frac{\partial v_{\text{rad}}}{\partial \lambda}, \quad (1)$$

where R represents the distance from the radar, v_{rad} is the one-dimensional Doppler velocity, and λ is the azimuth. Centered differencing is used.

The land-based radar will be supplemented by the TRMM Precipitation Radar, which measured the storm at a key time in the evolution of the intense cell of interest in this paper. TRMM composite images and scattering at 85 and 37 GHz will also be examined.

Strong convective cells within TS Gabrielle occurred between 0500 and 0900 UTC 14 September. The relevant ambient vertical wind shear computed at 0600 UTC is 271° at 13.3 m s^{-1} (Molinari et al. 2006), based on gridded analyses from ECMWF. Two independent estimates for the same hour from the Statistical Hurricane Intensity Prediction Scheme (SHIPS) database (DeMaria et al. 2005) give 267° at 11.4 m s^{-1} and 278° at 11.3 m s^{-1} . Each of the three estimates indicates large shear magnitude ($>10 \text{ m s}^{-1}$) by the definitions of Corbosiero and Molinari (2002) and Molinari and Vollaro (2010), and a virtually identical direction of ambient shear. The ECMWF estimate will be used in this paper. Ambient shear estimates from global models come surprisingly close to those based on a near-core vertical wind shear in the few available studies (Eastin et al. 2006; Braun et al. 2006; Reasor et al. 2009).

The application of helicity concepts to tropical cyclones has been addressed by Molinari and Vollaro (2008, 2010) and Baker et al. (2009). Helicity in this paper is calculated from 0–3 km in the vertical using the expression of Davies-Jones et al. (1990). Molinari and Vollaro (2010) calculated cell motion following the procedure of Ramsay and Doswell (2005). Recent evidence suggests that tropical cyclone supercells might not move as strongly to the right as in midlatitudes (Eastin and Link 2009). In this paper a more conservative cell motion estimate will be used: that of the vector mean wind in the 0–6-km layer. This estimate produces about a 40% reduction in helicity values (McCaul 1991; Molinari and Vollaro 2008).

3. Vortex-scale evolution of Tropical Storm Gabrielle

Musgrave et al. (2008) studied the initial formation of TS Gabrielle on 9 September 2001. Gabrielle developed underneath a nontropical midtropospheric low that drifted westward from Florida to the Gulf of Mexico prior to storm formation. Musgrave et al. (2008) noted that without this feature, no tropical storm developed. Gabrielle thus contained qualities of a subtropical storm early in its history. The Musgrave et al. (2008) simulation ended on 13 September.

Tropical Storm Gabrielle never developed a closed eyewall prior to its landfall near Venice, Florida, at about 1200 UTC 14 September, and its convection remained asymmetric. Knupp et al. (2006) and Kim et al. (2009) examined the precipitation structure in TS Gabrielle over

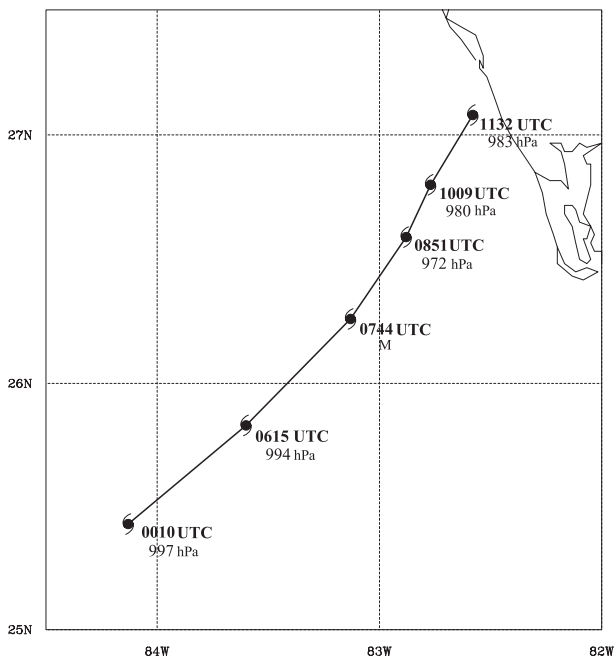


FIG. 1. Track of TS Gabrielle between 0000 and 1200 UTC 14 Sep 2001. The hurricane symbols indicate the locations of the D value minima at the times shown (bold) for each center crossing by U.S. Air Force reconnaissance aircraft. Accompanying each observation is the minimum central pressure estimate (hPa) from each flight (not available for the 0744 UTC crossing).

land. Sharp et al. (2002) studied the occurrence of tornadoes over Florida when the storm center was near and over land.

In between the periods covered by the above studies, TS Gabrielle experienced a dramatic intensification. Minimum central pressure fell 22 hPa in less than 3 h prior to 0900 UTC 14 September. Figure 1 displays the track of the storm and estimates of minimum central pressure during a 12-h period that includes the rapid intensification. The best track from the Tropical Prediction Center was not

used in this figure because its 6-hourly resolution was too coarse. Instead, the track in Fig. 1 gives the locations of minimum D value (i.e., minimum height of the flight-level pressure surface) for each center crossing by U.S. Air Force reconnaissance aircraft. The crossing at 0744 UTC appeared to show the original center plus a new circulation developing nearby (Molinari et al. 2006); the original center is plotted in Fig. 1. No central pressure estimate was available at that time. Figure 1 reveals a weak tropical storm that intensified suddenly and dramatically, then weakened somewhat prior to landfall. Using 6-hourly best-track wind data, TS Gabrielle intensified by 12.9 m s^{-1} in 24 h (1200 UTC 13 September–1200 UTC 14 September), which fits one of the rapid intensification criteria used by Kaplan and DeMaria (2010). The intensification rate of the storm was likely even larger, because minimum central pressure occurred near 0900 UTC 14 September, intermediate to the best-track values.

Table 1 compares the composite RI parameters of Kaplan and DeMaria (2010) for 12.9 m s^{-1} deepening per 24 h to non-RI values from the same authors and to the same parameters in TS Gabrielle. All except PER are averaged over the 24-h period of RI. PER represents a 12-h intensity change just before the 24-h period of interest. Two parameters were more favorable in TS Gabrielle than for standard RI: larger 200-hPa divergence and a greater deficit from maximum potential intensity. But the remaining six parameters took on less favorable values in TS Gabrielle than in standard RI. Two of these, vertical wind shear and cold cloud asymmetry, were even less favorable than those of the non-RI events in Table 1. There appear to be fundamental differences between the RI in TS Gabrielle and the statistical means found by Kaplan and DeMaria (2003, 2010). The nature of this asymmetric RI will be investigated in this paper.

TABLE 1. Comparison of parameters from the study of Kaplan and DeMaria (2010) to the same values in TS Gabrielle. The Kaplan and DeMaria (2010) Atlantic basin mean and standard deviation during deepening of 12.9 m s^{-1} in 24 h are given in the second column, the same values for non-RI cases are given in the third column, and the TS Gabrielle values are shown in the fourth column. All fields except PER are averaged over 24 h; in TS Gabrielle that represents the mean between 1200 UTC 13 Sep and 1200 UTC 14 Sep 2001. Kaplan and DeMaria (2010) provide the averaging areas over which each parameter is calculated.

RI parameter from Kaplan and DeMaria (2010)	RI mean (std dev)	Non-RI mean (std dev)	TS Gabrielle RI value
SHRD: 850–200-hPa ambient vertical wind shear (m s^{-1})	5.4 (2.4)	8.2 (4.2)	10.2*
SDBT: Cold IR cloud asymmetry ($^{\circ}\text{C}$)	13.7 (6.0)	16.9 (6.7)	22.5*
PX30: % area with cloud top $T < -30^{\circ}\text{C}$	76.6 (20.9)	57.8 (27.4)	60.0
RHLO: 850–700-hPa ambient relative humidity	73.1 (6.2)	68.7 (6.9)	71.0
OHC: Ocean heat content kJ cm^{-2}	55.4 (31.7)	36.9 (28.3)	43.0
PER: Deepening over the previous 12 h (m s^{-1})	4.0 (4.4)	1.3 (4.3)	2.6
D200: 200-hPa divergence (10^{-7} s^{-1})	46.9 (28.8)	24.7 (31.3)	56.0
POT: Deficit of the storm from its MPI (m s^{-1})	40.6 (12.5)	35.5 (13.9)	57.6

* Values more hostile to deepening than those in non-RI storms.

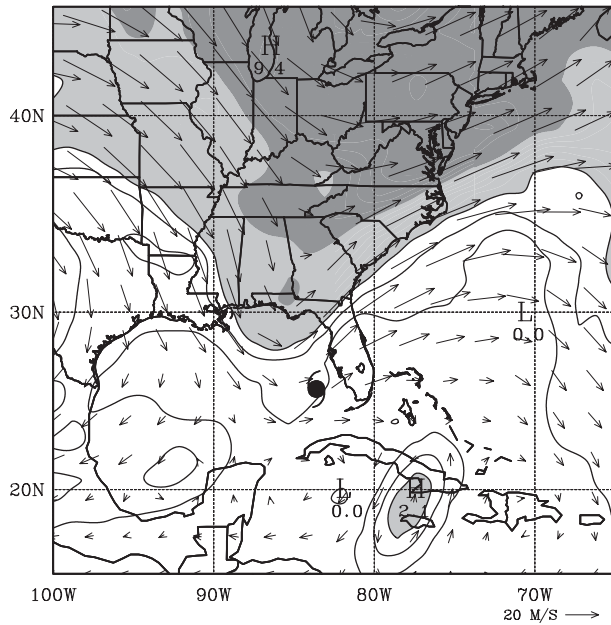


FIG. 2. Potential vorticity and wind on the 350-K isentropic surface. This surface lies between 175 and 225 hPa in the vicinity of the hurricane. Potential vorticity is contoured from 0 to 1.5 PVU in increments of 0.5 PVU ($1 \text{ PVU} \equiv 10^{-6} \text{ m}^2 \text{ K s}^{-1} \text{ kg}^{-1}$) and is shaded for higher values. The light and dark shading regions begin at 1.5 and 5 PVU, respectively.

An approaching midlatitude upper-tropospheric trough played a key role in the storm evolution. Molinari et al. (2006) found that the eddy angular momentum flux convergence criterion for a significant trough interaction (Hanley et al. 2001) was met during all 6-h periods on 14 September. Figure 2 displays a potential vorticity map on the 350-K isentropic surface at 0600 UTC 14 September. Molinari et al. (2006) provided similar maps at 0000 and 1200 UTC. Molinari et al. (2006) used an adiabatic balanced model to show that the approach of the trough produced a steady increase in both balanced and observed outflow at 200 hPa (and thus mean upward motion in the storm) between 0000 and 1200 UTC 14 September. The approach of the trough was accompanied by an increase in ambient vertical wind shear as well. As noted in section 2, wind shear was from the west at 13.3 m s^{-1} at the time of Fig. 2.

Figure 3 displays reflectivity from the WSR-88D radar at Tampa at 0741 UTC 14 September. The storm center implied by the cyan wind barbs (see discussion below) lies about 150 km from the radar. At that distance, and for the 0.5° elevation angle shown, the center of the radar beam lies at about the 3-km level (Klazura and Imy 1993). The influences of vertical wind shear and the upper trough created a strongly asymmetric precipitation field in TS Gabrielle. Almost all the precipitation lay in the downshear-left quadrant. No deep convection existed

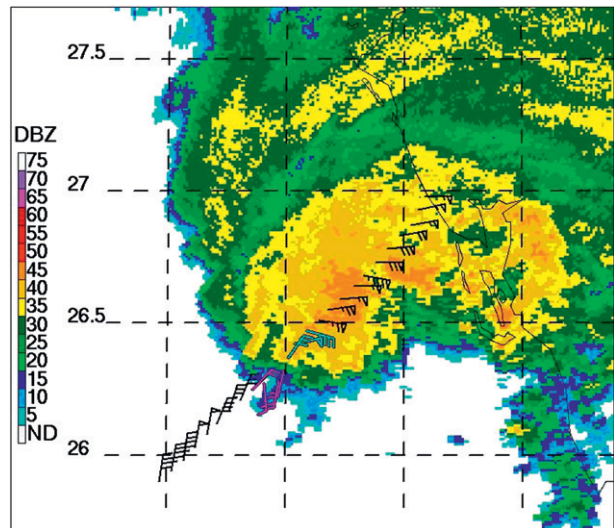


FIG. 3. Reflectivity for the 0.5° elevation angle from the Tampa WSR-88D radar at 0741 UTC 14 Sep 2001. Ambient vertical wind shear is from the west. Wind barbs represent storm-relative reconnaissance aircraft winds at 850 hPa every minute (about 6 km) from 0728 to 0754 UTC. Magenta wind barbs bracket the center of circulation; cyan wind barbs reveal an apparent second center developing within the downshear precipitation. The intense cell developed (i.e., lightning began) northeast of the second center about 20 min later.

upshear (see infrared satellite images in Molinari et al. 2006, their Figs. 6–9).

Also plotted in Fig. 3 are 850-hPa winds from U.S. Air Force reconnaissance aircraft from 0728 to 0754 UTC, in 1-min (roughly 6 km) increments. The storm motion has been subtracted, so that the wind barbs represent storm-relative winds. High wind speeds and strong inflow existed within the precipitation shield downshear left of the original center (magenta wind barbs). Weaker winds and outflow were present upshear right in the region without deep clouds. A second center of circulation (cyan wind barbs) appeared to be developing downshear left of the original center. About 90 min earlier at 0615 UTC, aircraft reconnaissance reported a broad, ill-defined center. Figure 3 suggests that 0741 UTC represented a key transition to a new center within the downshear precipitation.

Figure 4 displays the distribution of cloud-to-ground lightning with respect to the center of TS Gabrielle for three periods on 14 September: 0500–0629 UTC (green), 0630–0759 UTC (blue), and 0800–0859 UTC (red). Several aspects of this distribution are striking: (i) lightning was restricted to a narrow region left of downshear; (ii) lightning shifted inward with time against the ambient shear vector; (iii) the inward shift occurred discretely in the form of three separate cells developing progressively closer to the center; and (iv) the final cell formed northeast of the center near the 25-km radius,

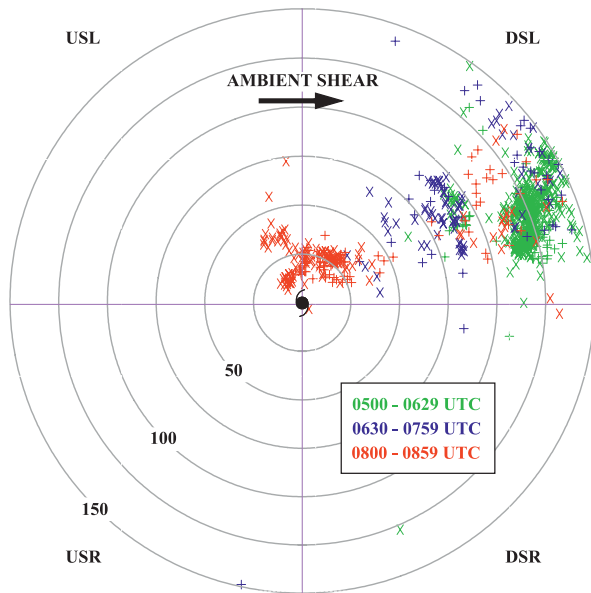


FIG. 4. Cloud-to-ground lightning locations with respect to the reconnaissance-based storm center. Flashes lowering positive and negative charge to ground are indicated by the symbols + and x, respectively. Green, blue, and red flashes represent the time periods shown on the figure. DSL and DSR represent downshear left and right, respectively; USL and USR are the analogous upshear quadrants. The range ring labels are given in km.

adjacent to the developing circulation center shown in Fig. 3. The lowest pressure in the storm prior to landfall occurred at 0851 UTC during the lifetime of the last cell. It will be seen in the following sections that this cell was one of the most intense ever observed in tropical cyclones.

Molinari and Vollaro (2008, 2010) noted the substantial enhancement of helicity and CAPE downshear of tropical cyclones experiencing large ambient shear. They used the energy helicity index (EHI), a normalized product of helicity and CAPE, to measure the likelihood of severe cells. In TS Gabrielle, few data exist to evaluate these variables in the vicinity of the strong cells in Fig. 4. The nearest ECMWF model grid point in time and space to the development of the intense cell shown in red in Fig. 4 was found just downshear left of the center at 0600 UTC 14 September. That grid point exhibited CAPE of 1162 J kg^{-1} and helicity of $31 \text{ m}^2 \text{ s}^{-2}$, giving a small EHI of about 0.2. Although this would not likely support a supercell, the global model lacks resolution and might not be representative. The nearest sounding to the cell is the Tampa, Florida, sounding at 1200 UTC, which lies about 60 km downshear left of the center, about the same relative location as the cell 3 h before. Helicity at that time reached $795 \text{ m}^2 \text{ s}^{-2}$, an exceptionally large value. CAPE was nearly zero, and the resulting EHI was again not supportive of severe

cells. But this point lies over land, where the air was unusually cool (Knupp et al. 2006) and not representative of air over the Gulf of Mexico near the storm.

Another source exists for CAPE and helicity calculations. Sharp et al. (2002) simulated TS Gabrielle using the Advanced Regional Prediction System (ARPS) Data Analysis System (ADAS) high-resolution analysis/simulation system (10- and 2-km inner-nested grid spacings) that contains much higher resolution and better model physics than the ECMWF model. Although Sharp et al. (2002) were focusing on supercells over land, their analysis region included the downshear-left quadrant adjacent to the storm center at 0900 UTC 14 September. The strong cell in TS Gabrielle formed in that region about one hour earlier. CAPE values over water in their analyses at 0900 UTC exceeded 1500 J kg^{-1} downshear of the center, in the same region where helicity exceeded $300 \text{ m}^2 \text{ s}^{-2}$. Even after adjustment for a more conservative cell motion estimate (see section 2), their analyses indicated $\text{EHI} > 1$ downshear of the storm, which supports the existence of severe cells (Hart and Korotky 1991).

The environment of TS Gabrielle before and during its rapid intensification can be summarized as follows:

- A trough approached from the northwest, producing large ambient vertical wind shear, but also stronger forced upward motion (Molinari et al. 2006).
- In response to the vertical wind shear, precipitation became strongly asymmetric, occurring almost exclusively in the downshear-left quadrant.
- Based on the Sharp et al. (2002) simulation, helicity and CAPE were large enough in the downshear-left quadrant to support the existence of intense cells. The strongest wind speeds measured in the storm were located in the same region.
- Three long-lasting convective cells developed in the downshear-left quadrant, each progressively closer to the center with time, between 0500 and 0900 UTC.
- The last of the three cells developed near the storm center. During the life of this cell, reconnaissance aircraft reported 972-hPa minimum sea level pressure, 22 hPa lower than 2.5 h before.

In the following section the evolution of this cell will be examined in detail.

4. Evolution of an intense cell during rapid intensification

Figure 5 reexamines the lightning from the third cell in Fig. 4 by using 10-min increments, beginning at 0801 UTC and ending 50 min later. The colored circles indicate the mean locations of lightning flashes

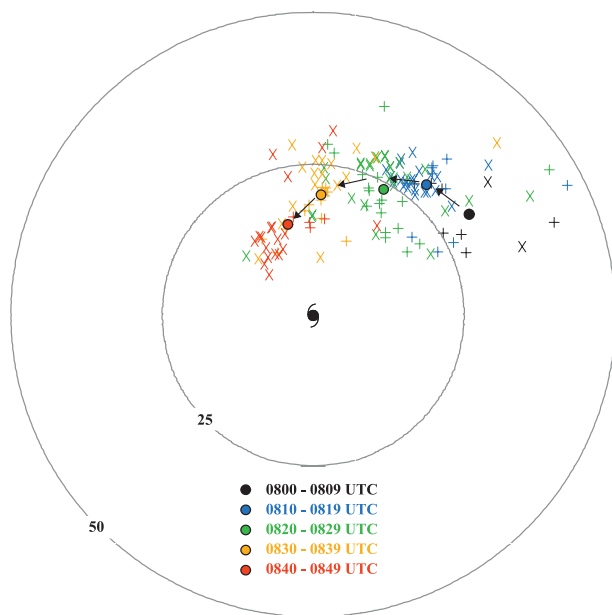


FIG. 5. Cloud-to-ground lightning locations as in Fig. 4, but only for the innermost cell in 10-min increments. Each period is shown in a different color as indicated. Colored circles represent the mean location of lightning flashes within each 10-min period. The range ring labels are given in km.

during each 10-min period. The cell moved cyclonically and inward with respect to the tropical storm center. Its average speed of motion over the 50-min period was 14.5 m s^{-1} . Lightning ended shortly after the cell moved into the upshear half of the circulation, consistent with other sheared storms (e.g., Heymsfield et al. 2001). Lightning appears to reveal the evolution of strong updrafts better than radar reflectivity, because large reflectivity can continue to exist upshear in falling rain after updrafts have ended.

Figure 6 displays the evolution of radar reflectivity over the same period as Fig. 5, starting at 0801 UTC, just prior to the outbreak of significant lightning. These images cover a much smaller region than Fig. 3 in order to focus on the cell evolution. Also shown are 10 min of cloud-to-ground lightning flashes centered on the time of each radar image, and the location and diameter of mesocyclones determined using the WSR-88D algorithm (Stewart and Lyons 1996; NOAA 2006). At 0801 UTC (Fig. 6a), the extensive downshear precipitation shield resembled that from 20 min earlier (Fig. 3). Little lightning was present. No clear sign of cyclonic curvature existed within the reflectivity. Ten minutes later (Fig. 6b), a cluster of lightning flashes developed within a region of reflectivity above 45 dBZ. The lightning flash rate increased during the period centered on 0821 UTC (Fig. 6c). Ten minutes later, as frequent lightning continued, the mesocyclone algorithm

was triggered. The mesocyclone extended in the vertical from 2.0 to 6.3 km, and exhibited an elliptical shape in the horizontal that extended $22.8 \times 15.4 \text{ km}$. It contained maximum shear vorticity (i.e., from the Doppler winds) of $2.2 \times 10^{-2} \text{ s}^{-1}$, and visual evidence of rotation in the reflectivity field was much greater than 10 min before.

The size of this mesocyclone indicates that it is nothing like those that appear in tropical cyclone supercells, in which mesocyclones are typically 2–8 km in diameter (e.g., Eastin and Link 2009; Baker et al. 2009; McCaul et al. 2004). The algorithm was activated because the symmetry, Doppler velocity difference, maximum vorticity, and vertical coherence criteria for a mesocyclone were met. Subsequently this feature will be referred to as the *inner-core vortex* to avoid misleading terminology. One relevant question is whether this feature represents the cell or the tropical cyclone itself. The answer to this question will become apparent in later figures.

By 0841 UTC (Fig. 6e), the inner-core vortex extended from 1.9 to 6.3 km in the vertical, and was nearly circular in the horizontal with a diameter of 23 km. A hook echo was present and the reflectivity field strongly resembled the supercell schematic of Lemon and Doswell (1979). Lightning had become less frequent at this time. By 0851 UTC (Fig. 6f), the weak echo region filled in somewhat and the hook was less well defined. The inner-core vortex extended through almost the same layer as before and had grown laterally to $28.7 \times 23.7 \text{ km}$. A second smaller vortex existed to the northeast. Lightning within the cell had ended by this time. Figure 6f also records the path of a U.S. Air Force reconnaissance aircraft that passed near the center at the same time. Data from this flight will be examined later in this section.

Figure 7 gives one-dimensional vorticity from the Doppler radial velocity plotted on the same reflectivity fields as in Fig. 6, but on a cylindrical grid centered at the position of the radar. Reflectivity contours vary slightly from Fig. 6 as a result of interpolation. Only two vorticity contours are plotted: 0.5 and $1.5 \times 10^{-2} \text{ s}^{-1}$. Small transient regions of vorticity greater than $0.5 \times 10^{-2} \text{ s}^{-1}$ existed at 0801, 0811, and 0821 UTC (Figs. 7a–c). Yet only 10 min later at 0831 UTC (Fig. 7d), maximum vorticity reached $2.2 \times 10^{-2} \text{ s}^{-1}$, at the same time that the mesocyclone algorithm was triggered. This dramatic increase occurred on the southwest (downwind) end of the region of strongest radar reflectivity gradient. Shapiro and Willoughby (1982) found maximum vorticity generation in a symmetric vortex within the region of diabatic heating gradient. To the extent that the reflectivity gradient represents a comparable gradient in diabatic heating, the observed increase in vorticity might represent an asymmetric analog to the results of Shapiro and Willoughby (1982).

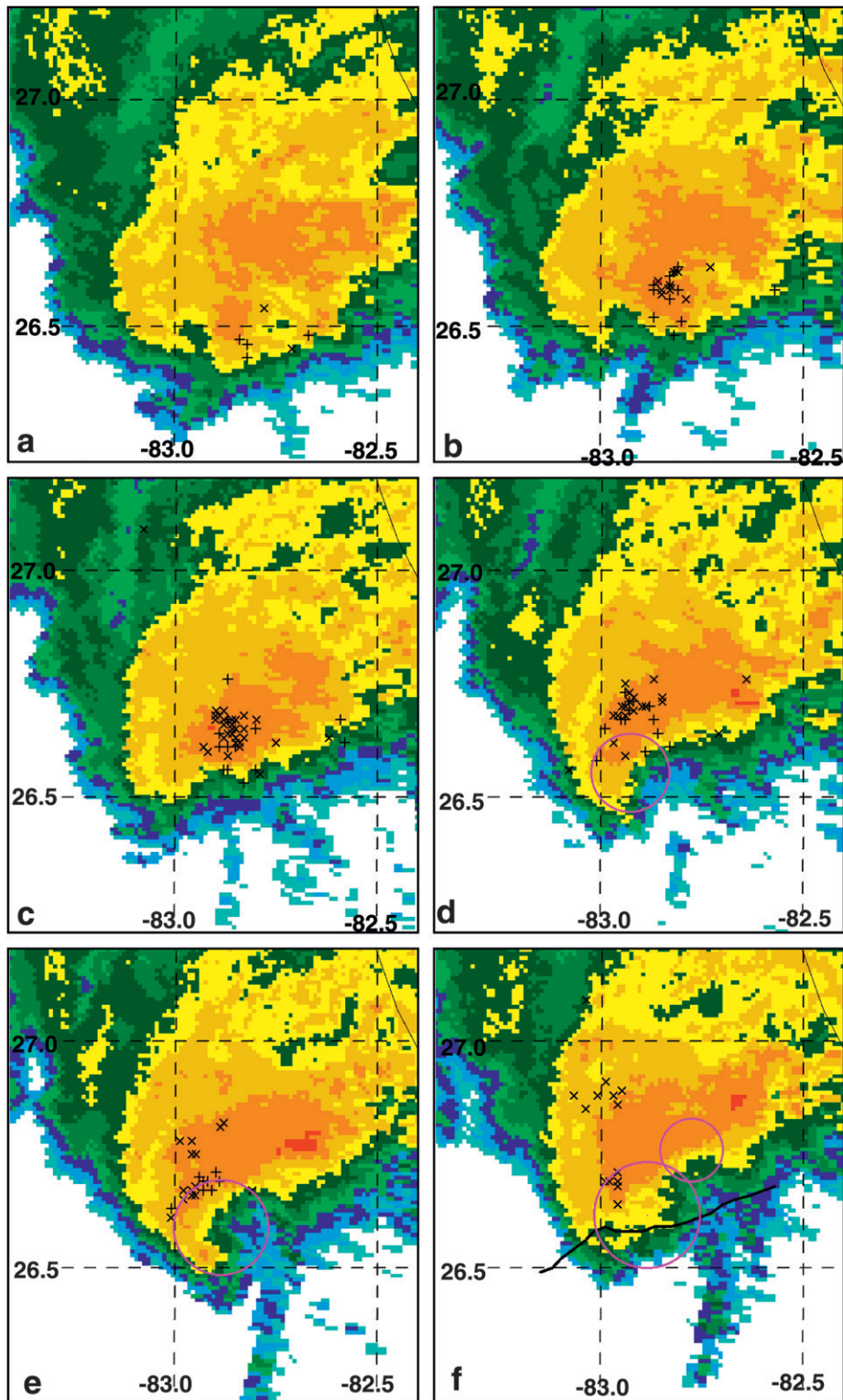


FIG. 6. Radar reflectivity as in Fig. 3, starting 20 min later in 10-min increments, and over a smaller (1° latitude–longitude) region. Also shown are cloud-to-ground lightning locations (x: negative flashes; +: positive flashes) for 10-min periods centered on the time of each radar image. Circles indicate mesocyclones defined using the operational Doppler radar algorithm (NOAA 2006) at (a) 0801, (b) 0811, (c) 0821, (d) 0831, (e) 0841, and (f) 0851 UTC. In (f) the path of a reconnaissance flight that came nearest to the center at 0850 UTC is shown. Ambient vertical wind shear is from the west.

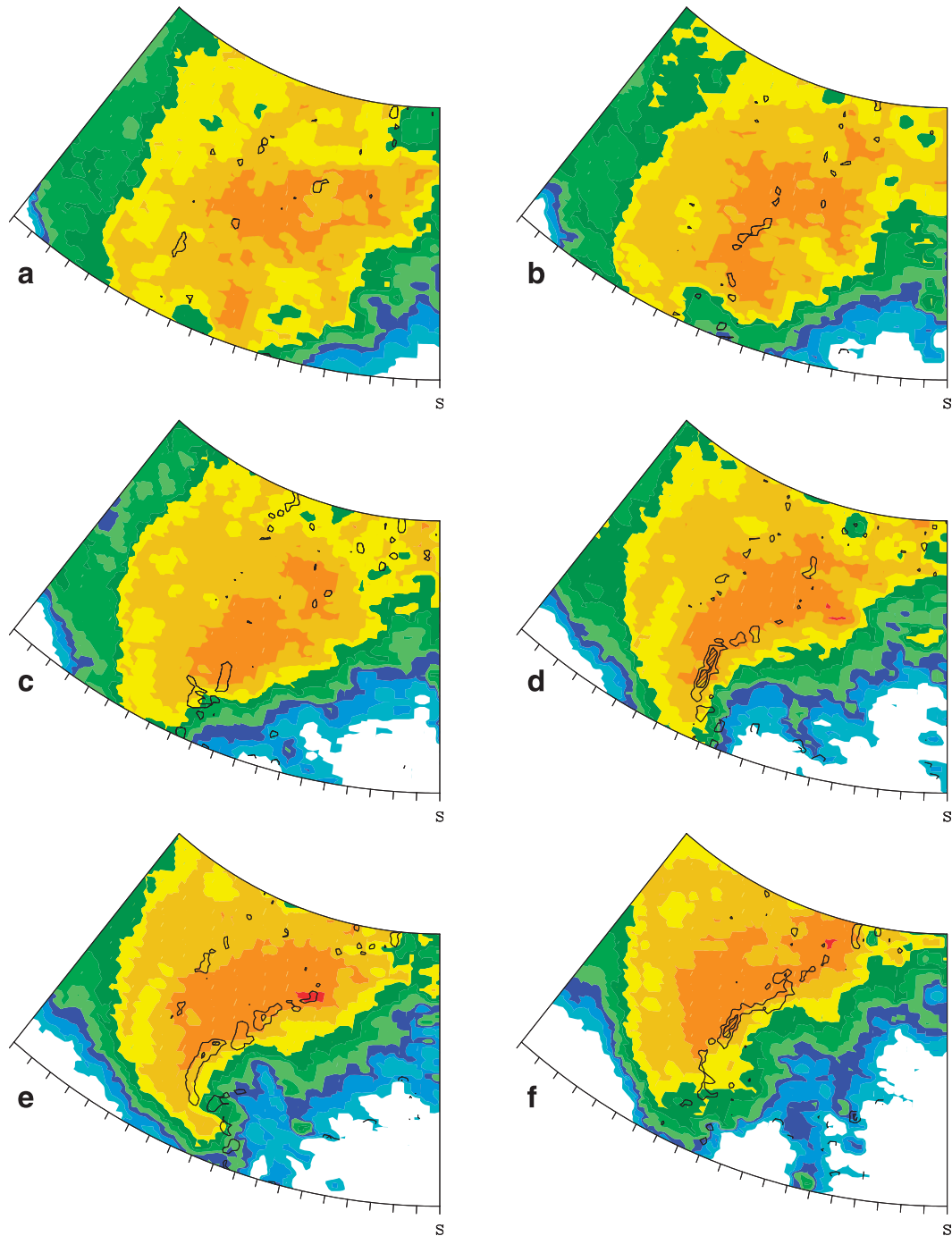


FIG. 7. Radar reflectivity for the same times as in Fig. 6, but plotted over a portion of the cylindrical grid centered on the radar. Also shown is the one-dimensional vertical vorticity calculated from the radar Doppler velocity [Eq. (1) in the text]. All fields are from data at the 0.5° elevation angle of the radar. Vorticity contours only for $+0.5$ and $1.5 \times 10^{-2} \text{ s}^{-1}$. Heavy contours and hatching indicate vorticity above $1.5 \times 10^{-2} \text{ s}^{-1}$.

By 0841 UTC (Fig. 7e), maximum vorticity had decreased to $1.8 \times 10^{-2} \text{ s}^{-1}$, but large vorticity values extended all along the reflectivity gradient. By 0851 UTC (Fig. 7f), maximum vorticity had shifted northward with the storm and increased again to $2.1 \times 10^{-2} \text{ s}^{-1}$. A

second vorticity maximum was present northeast of the first, associated with the second mesovortex in Fig. 6. As before, the maximum vorticity tended to occur within or downwind of the region of maximum radar reflectivity gradient. The value of the vorticity maximum exceeded

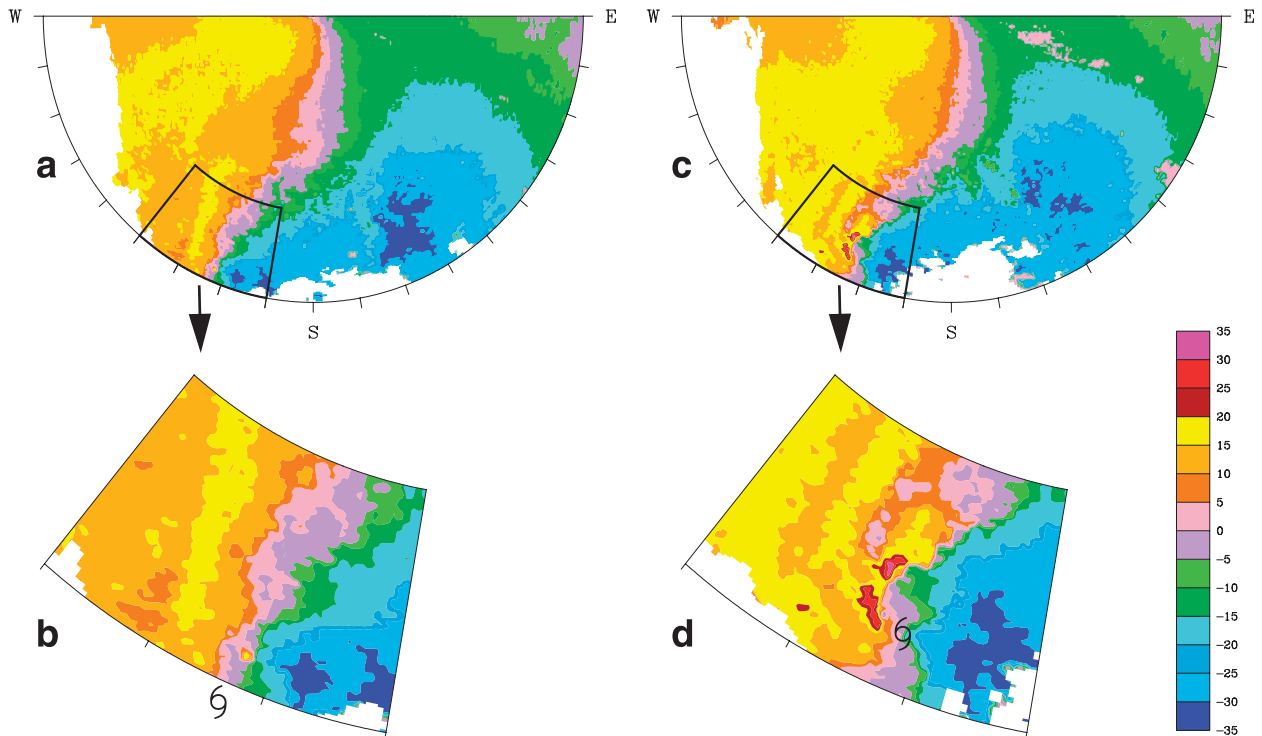


FIG. 8. Radial velocity (m s^{-1}) from the Tampa radar at the 0.5° elevation angle. (top) The broader tropical storm circulation out to the 147 km radius at (left) 0816 and (right) 0841 UTC. (bottom) An expanded view. The tropical storm symbol indicates the position of the interpolated reconnaissance-based center. Warm colors represent outflow from the radar [located at the top center of (a) and (c)] and cool colors represent inflow. The radar beam is centered near the 3-km level at the bottom edge of the plots.

that found in a simulation of rapid intensification by Rogers (2010) by a factor of 3. This provides another measure of the intensity of the cell. Little evidence of vorticity maxima existed southeast of the inner-core vortex at any time shown in Fig. 7, suggesting the possibility of an azimuthal wavenumber-1 vorticity pattern.

The features in Figs. 6 and 7 resemble those seen previously in tropical cyclones. Zipser and Gautier (1978, their Fig. 8) showed a schematic radar reflectivity structure and small vortex similar to that in Fig. 6e in a forming tropical depression. Although it was a much stronger storm, Hurricane Guillermo contained a hooklike feature at the downwind end of the eyewall (Sitkowski and Barnes 2009, their Fig. 5). Simpson et al. (1997) examined the genesis of Tropical Cyclone Oliver (1993) during a period that an eye developed. The storm contained a reflectivity maximum in the core associated with a hot tower at the downwind end of a crescent-shaped, azimuthal wavenumber-1 pressure minimum (their Fig. 9). Although vorticity was not given, balanced dynamics argues for a strip of cyclonic vorticity coincident with this feature. Its structure would then resemble Figs. 6d–f in this paper. Vertical wind shear in TS Oliver calculated from ECMWF analyses was from 240° at 10 m s^{-1} . Adjusting for this Southern Hemisphere storm (where

downshear right is equivalent to downshear left in the Northern Hemisphere), TS Oliver closely resembled TS Gabrielle. It is argued that Oliver might have intensified in a similar manner.

Figure 8 displays the one-dimensional Doppler radial velocity in TS Gabrielle from the Tampa radar for the 0.5° elevation angle, representing approximately the 2.5–3-km elevation near the storm center. Two times are shown: 0816 and 0841 UTC. At each time, the broad radar radial velocity field is shown in the top panel, and an expanded view near the storm center in the bottom panel. The zero isodop lies between the pink and violet shading. These plots give a picture of how the broader tropical storm, the inner-core vortex, and the cell coexisted.

Figure 8a (0816 UTC; top-left panel) shows a broad tropical storm circulation at larger radii from the storm center (as seen in the yellow shading for strong flow away from the radar, and dark blue shading for strong flow toward the radar). Lightning in the cell has been active for about 5–10 min at this time. Although the mesocyclone algorithm had not yet been activated, a second wind maximum had already developed at smaller radii, indicated by the separate regions of yellow and dark blue shading near the storm center. This suggests that the cell had already helped to produce some

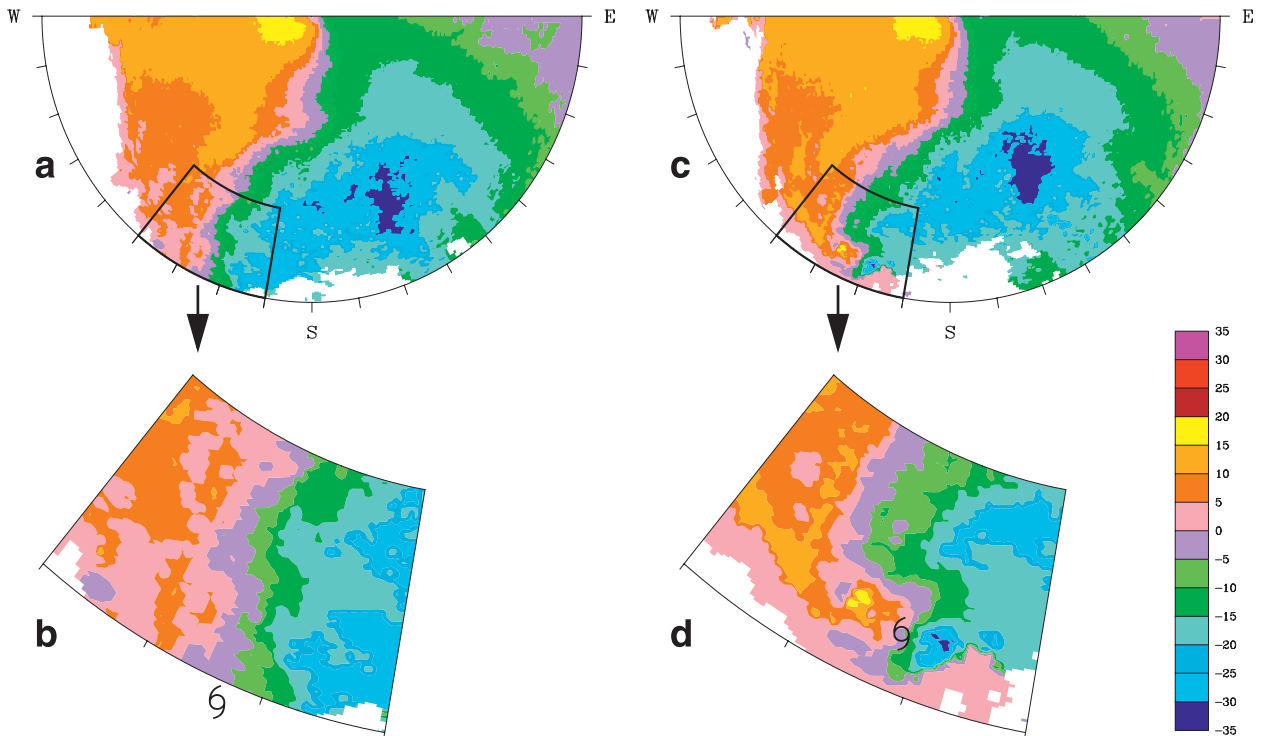


FIG. 9. As in Fig. 8, but for the 1.5° elevation angle, which samples near the 5-km level at the storm center.

intensification of the new vortex downshear shown by the cyan wind barbs in Fig. 3.

Figures 8c,d (right panels) reveal the circulation at 0841 UTC, after the cell had been active for more than 30 min. Some acceleration of the broader circulation occurred northwest of the center, but the major changes from 25 min earlier occurred as the inner-core vortex intensified (Fig. 8d), producing Doppler wind maxima that exceeded 30 m s^{-1} on either side of the center at about the 10–12-km radius.

Figure 9 gives the same sequence as Fig. 8, but for the 1.5° elevation angle, which represents approximately the 5-km level at the location of the storm center. The Doppler velocities weakened upward at both times. Using the tropical storm symbol as a marker, it is apparent that the inner-core vortex at 0841 UTC is almost completely upright (cf. Figs. 8d and 9d). The broader vortex, however, has a substantial tilt. In the lower troposphere (Fig. 8d), the zero isodop extends north-northeastward from the center. In the midtroposphere (Fig. 9d), the zero isodop in the broader vortex is shifted northward and westward, or approximately left of the ambient shear vector.

Figures 8 and 9 support the findings of Riemer et al. (2010). They found in a simulated tropical cyclone experiencing large ambient shear that the inner-core vortex had a much smaller tilt than the outer vortex. They attributed

the broad asymmetry in precipitation outside the core to the tilt of the outer vortex, with maximum precipitation in the direction of the outer vortex tilt. Figures 6e,f of this paper show a broad precipitation shield north of the center, consistent with the findings of Riemer et al.

The TRMM satellite made an overpass of TS Gabrielle at 0840 UTC 14 September, virtually coincident with Figs. 6e, 7e, 8c,d, and 9c,d. Lee et al. (2002) described the interpretation of TRMM data in tropical cyclones. Figure 10 presents the 37-GHz composite image. The concentrated intense convection (red shading) just east of original center shows clearly. Cyan regions over water give evidence of low cloud swirls west (upshear) of the storm center. The microwave scattering signature in the most intense part of the cell was exceptional. This scattering is measured by the polarization-corrected brightness temperature (PCT; Mohr and Zipser 1996) at both 85- and 37-GHz frequencies. The 85-GHz minimum PCT in the Gabrielle cell at 0840 UTC was 63 K (D. Cecil 2009, personal communication). A collection of 127 000 TRMM “precipitation features” from tropical cyclones puts the Gabrielle cell 85-GHz PCT in the top 0.007% (H. Jiang 2009, personal communication). The 37-GHz PCT of 179 K was almost as exceptional. Such large scattering values are associated with frequent lightning, large ice content, and intense updrafts through a deep layer (Cecil et al. 2002, 2005).

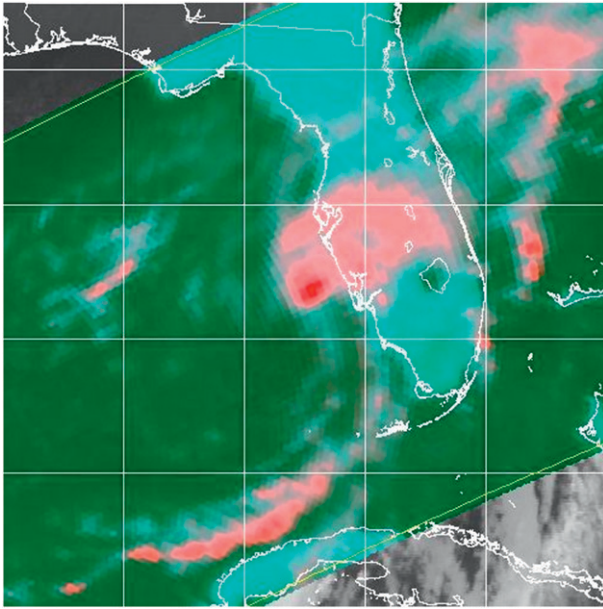


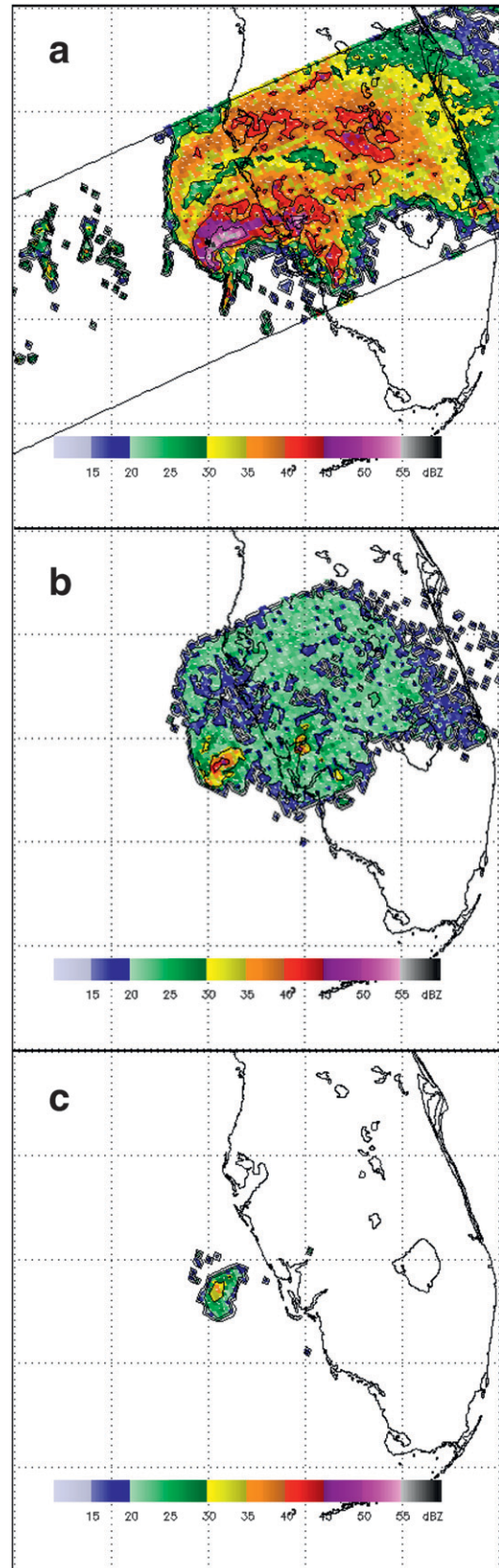
FIG. 10. 37-GHz composite at 0840 UTC 14 Sep 2001. Strongest convection is in red, less strong convection is in pink, and lower clouds over water are in cyan.

Figure 11 displays reflectivity at three levels from the TRMM Precipitation Radar for the same time as Fig. 10. Reflectivity near the surface exceeded 55 dBZ. The cyclonic banding of the reflectivity maxima indicates that a vorticity maximum had developed at the surface in association with this cell. Maximum reflectivity exceeded 45 dBZ at 7 km, and 35 dBZ at 12 km. Houze et al. (2009) described a cell in predepression Ophelia with reflectivity exceeding 40 dBZ at the 12-km height, and containing vertical motion above 10 m s^{-1} over a region 10 km deep and more than 10 km wide. The horizontal scale of the large reflectivity in Fig. 11 is comparable to that of the Ophelia cell at the 7- and 12-km elevations, suggesting that the cell in TS Gabrielle also contained broad updrafts through a deep layer. The 12-km reflectivity suggests that only a single updraft reached this level. This is similar to other intense cells measured by TRMM in tropical cyclones (Kelley et al. 2004). Kelley et al. found such deep cells isolated at the downwind end of bands of convection in the tropical cyclone core. The cell in TS Gabrielle fits this description.

Ten minutes after the TRMM overpass an Air Force reconnaissance flight at the 700-hPa level passed near the center along the path plotted in Fig. 6f. Figure 12 shows D value, temperature, and relative humidity



FIG. 11. Reflectivity (dBZ) from the TRMM precipitation radar at 0840 UTC 14 Sep 2001: (a) near surface, (b) 7-km elevation, and (c) 12-km elevation.



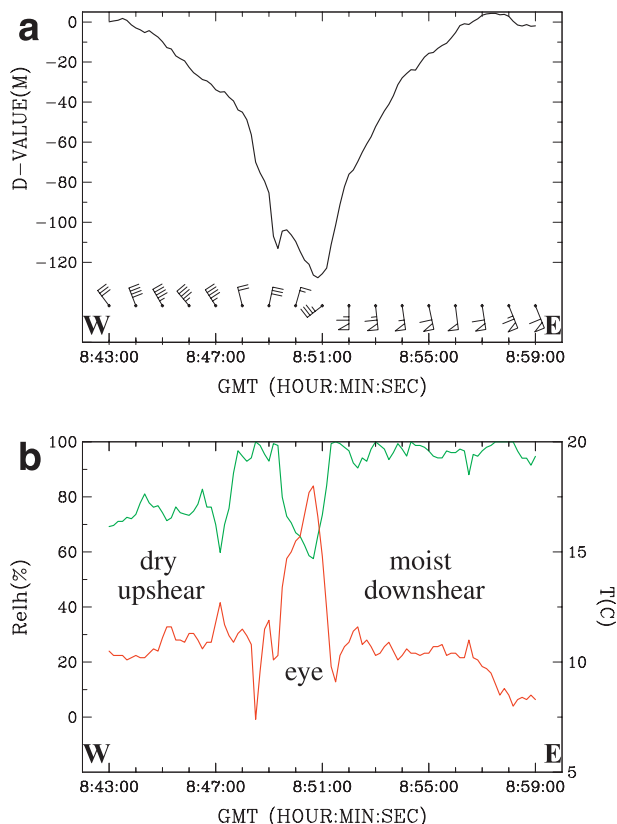


FIG. 12. U.S. Air Force reconnaissance data cross section at 700 hPa for the flight that crossed the center from west to east at 0851 UTC 14 Sep 2001. The flight track is given in Fig. 6f. (top) D value (700-hPa height minus standard atmosphere height). (bottom) Temperature ($^{\circ}\text{C}$, red) and relative humidity (% , green). Each minute represents about 6 km of distance; the plot extends about 48 km either side of the center.

extending about 48 km either side of the minimum pressure along this track. As seen in Figs. 6f and 7f, the track of the reconnaissance flight missed the regions of large vorticity and strong reflectivity. Nevertheless, this flight observed a 972-hPa minimum pressure. Assuming nearly balanced dynamics, pressure was likely substantially lower near the vorticity maxima in Figs. 7d–f.

Consistent with previous results (e.g., Shelton and Molinari 2009), Fig. 12 reveals saturated air downshear and unsaturated air upshear just outside the storm center. The most striking aspect of this cross section is the strong narrow warm core representing an eyelike feature. It was accompanied by a reduction of relative humidity of more than 40% from the saturation on either side of the warm core, strongly supporting the existence of subsidence. This temperature anomaly appears to represent a local enhancement of the warm core of the tropical storm adjacent to the cell.

Earlier it was asked whether the inner-core vortex represented the cell or the tropical storm itself. In some ways

the inner-core vortex seems to be directly associated with the cell. It developed adjacent to the cell (Fig. 8) and was associated with a strong local vorticity maximum (Fig. 7f) and a small intense warm core (Fig. 12). Conversely, the reconnaissance-based wind field at 700 hPa in Fig. 12 revealed that this warm core existed within what is clearly a broad (100 km) tropical storm-scale disturbance. Figures 8 and 9 showed a nearly upright inner vortex within a tilted outer vortex. This configuration is consistent with balanced dynamics of a tropical cyclone experiencing large ambient vertical wind shear (Riemer et al. 2010). It is argued that the cell, inner-core vortex, and broader tropical storm evolved in a coupled manner and are not easily separable.

Tropical Storm Gabrielle contained only the one strong cell near the core and one period of rapid deepening. After that period the storm was quasi-steady with little lightning prior to landfall. The storm remained asymmetric, and transient mesovortices were occasionally detected by the radar. The storm at this stage fit the description of Tropical Storm Allison given by Sippel et al. (2006): a broad cyclonic region with embedded small areas of larger vorticity and the lack of a clear-cut center location. The early stages of Tropical Storm Dolly (Reasor et al. 2005) had a similar structure.

A number of questions arise from this evolution. Of central interest are (i) whether the cell was a supercell; (ii) whether the cell caused the rapid deepening, or was simply part of the process; and (iii) the physical and dynamical mechanisms of this asymmetric rapid intensification. These issues will be addressed in the discussion.

5. Discussion

a. Was this a supercell?

The inner-core cell was unusually intense in terms of the depth of 30-dBZ radar return and scattering in the 37- and 85-GHz microwave channels, all of which fell within the top 0.2% of cells measured by TRMM in any location (i.e., land or ocean; Cecil et al. 2005). The structure of the lower-tropospheric radar image at 0841 UTC (Fig. 6e) strongly resembled the supercell schematic of Lemon and Doswell (1979, their Fig. 7). The presence of a hook and a weak echo region showed clearly. A distinct lightning signature lasted for 50 min (Figs. 4–6). The maximum one-dimensional vorticity met a supercell criterion from Bunkers et al. (2009) by exceeding $0.6 \times 10^{-2} \text{ s}^{-1}$ for more than 30 min (Fig. 7). The 700-hPa vorticity maximum was at least as large as those observed in offshore tropical cyclone supercells (Eastin and Link 2009). A mesocyclone defined by Doppler radar developed after about 20 min of continuous cloud-to-ground

lightning (Fig. 6), consistent with observations of mid-latitude cells (Shafer et al. 2000). CAPE and helicity in the region where the cell formed (Sharp et al. 2002) were comparable to those found in the vicinity of tropical cyclone supercells by Baker et al. (2009) and Eastin and Link (2009). The high correlation of vertical velocity and vertical vorticity in supercells (e.g., Weisman and Klemp 1984; Baker et al. 2009) could not be evaluated, nor could the extent of off-hodograph movement (e.g., Weisman and Rotunno 2000; Eastin and Link 2009).

Remaining evidence casts considerable doubt that this was a supercell. Supercells have their strongest vertical vorticity in midlevels, especially early in their lifetimes (Weisman and Klemp 1986). Wind speeds in TS Gabrielle, however, were strongest in the lower troposphere and decreased upward (Figs. 8 and 9). The mesocyclone detected by the radar was much larger than those observed in tropical cyclone supercells (e.g., Eastin and Link 2009). Reconnaissance aircraft flights only 10 min after the clear hook echo revealed a narrow warm core that almost certainly arose from subsidence (see Fig. 12). The weak echo region of a supercell does not contain subsidence. Finally, in the high-vorticity environment within the core of a hurricane, only a right-moving supercell would be expected. The observed cell moved inward, which is unlikely to be right of the mean wind in a tropical cyclone.

This cell is much more likely to fall into the general category of a vortical hot tower (VHT; Hendricks et al. 2004). Its lifetime and its maximum wind speed in the lower troposphere fit the simulations of Montgomery et al. (2006) and the observations of Houze et al. (2009) and Bell and Montgomery (2010), and are suggestive of a bottom-up development of the storm. The strong cell in TS Gabrielle resembled those shown by Kelley et al. (2004): single intense deep cells in the tropical cyclone core at the downwind end of convective bands. The TS Gabrielle cell also had properties of that given by Houze et al. (2009): maximum vorticity of order 10^{-2} s^{-1} , strong localized warming adjacent to the cell, and, based on the reflectivity structure in Fig. 11, broad deep updrafts. Recent work by Romps and Kuang (2010) strongly suggests that fusion heating is responsible for these broad updrafts reaching the tropopause. The presence of exceptional 85-GHz scattering, indicating large ice content, also indicates strong fusion heating. The cells described in this paper and by Houze et al. (2009) might be unique to the high-moisture, large-vorticity environment of the tropical cyclone core.

b. Nature of asymmetric RI

Figure 3 revealed what appeared to be a key transition in TS Gabrielle. At that time (0741 UTC), a new

circulation center was apparently forming within the downshear precipitation shield. Only after this reformation did a strong cell develop just downshear left of the new center. As noted above, the cell likely produced large fusion heating in the mid- and upper troposphere, based on both the huge TRMM 85-GHz scattering and the reasoning of Romps and Kuang (2010). Nolan et al. (2007) showed that KEE reached its largest values at inner radii at elevations of 6–10 km. The strong cell was thus perfectly structured and well placed to contribute to rapid intensification of the storm. Evidence for the efficient creation of kinetic energy by heating within the cell is present in the rapid growth of wind and vorticity in the core revealed by Figs. 7 and 8. Support for the large efficiency of conversion of heating to warming (Vigh and Schubert 2009) showed in the reconnaissance cross section in Fig. 12: a strong localized warm core adjacent to the cell (see Figs. 6f and 7f) and on a similar scale to the cell, coincident with the location of the minimum central pressure.

Even though the simulations of Nolan (2007) contained no ambient vertical wind shear, some insight can be gained by direct comparison with his results. In his simulation, azimuthal mean vorticity in the boundary layer inside the 10-km radius grew by almost a factor of 3 in a single hour, from 1.2 to $3.1 \times 10^{-3} \text{ s}^{-1}$. Figure 7 of this paper indicated rapid vorticity growth in TS Gabrielle. In both Nolan's simulation and TS Gabrielle, this vorticity growth occurred in the presence of heating at small radii. An x - y plot of lower-tropospheric vorticity (Fig. 18 from Nolan 2007) displayed a single maximum about 10 km outside of the center of circulation, not unlike the structure in Fig. 7d. Finally, Nolan's (2007) inner-core vortex developed quickly as a separate wind maximum within a broader wind field of about 15 m s^{-1} at the 55-km radius, much like Figs. 8 and 9 of this paper. Tropical Storm Gabrielle differed in that both the heating and the related vorticity were much larger, the storm was more asymmetric, and the intensification was more rapid but also more brief.

One apparent role of the ambient vertical wind shear in this process was to promote the growth of a strong cell by maximizing the favorable anomalies of vertical motion, inflow and inflow depth, helicity, CAPE, and local shear in the downshear-left quadrant (Molinari and Vollaro, 2008, 2010; Black et al. 2002), especially near the center (Eastin et al. 2005; Braun and Wu 2007). The sequence of events for RI is seen as follows: (i) strong vertical wind shear produced persistent downshear rainfall and subsequent downshear vortex redevelopment within the precipitation shield (Fig. 3), (ii) the tilting of this new vortex by the ambient shear created favorable conditions for a strong cell to develop downshear in the

storm core (e.g., Eastin et al. 2005; Braun and Wu 2007), and (iii) this cell dramatically enhanced the heating in the region of large KEE (Nolan 2007) and contributed to subsequent rapid intensification of the storm. This process provides a mechanism for asymmetric rapid intensification. It is argued that the rapid intensification occurred *because of* the ambient shear, not *in spite of* the ambient shear. This fits the arguments made by Reasor and Montgomery (2001), who noted that if downshear convergence and convection were larger than could be produced by symmetric mechanisms alone, intensification could be accelerated by the presence of vertical wind shear. Based on Table 1 shown earlier, such storms might be expected to have strongly unfavorable ambient vertical shear and deep-cloud symmetry, but otherwise have relevant parameter values that fall within a standard deviation of those found for RI by Kaplan and DeMaria (2003, 2010).

These arguments raise the question as to why all strongly sheared storms do not rapidly intensify by the same process. For instance, TS Chantal (2001) experienced almost identical vertical wind shear magnitude to TS Gabrielle, exhibited a similar horizontal structure (Heysfield et al. 2006), and contained several strong cells. Yet Chantal did not experience RI. It is speculated that in TS Gabrielle the approach of an upper-tropospheric trough was a key factor in allowing this sheared storm to intensify rapidly. The upward motion associated with the trough (Molinari et al. 2006) would in principle contribute to the increase in CAPE and helicity associated with stronger radial-vertical flow (Molinari and Vollaro 2010), and thus make a strong, long-lasting downshear cell more likely. This hypothesized role of the upper trough is consistent with the observation by Kaplan and DeMaria (2003) that large inward eddy fluxes of angular momentum often accompanied RI when symmetry conditions were not met. Such fluxes usually indicate the approach of an upper-tropospheric trough (e.g., Molinari and Vollaro 1989).

The symmetric dynamics of tropical cyclone intensification, including the role of unbalanced boundary layer flow, has been clearly described by Smith et al. (2009). Even storms with small ambient shear have asymmetric structure during deepening in the form of VHTs (Eastin et al. 2005; Montgomery et al. 2006; Nolan 2007; Rogers 2010). But the RI in TS Gabrielle took a different form: a single intense cell interacting with a primary vortex in the presence of highly asymmetric clouds and precipitation and large ambient shear. The detailed dynamics of this asymmetric RI remains to be fully understood.

Acknowledgments. We are indebted to John Kaplan of the Hurricane Research Division of NOAA for providing

calculations of the rapid intensification parameters for TS Gabrielle used in Table 1. We also thank Dr. Daniel Cecil of the University of Alabama in Huntsville and Dr. Haiyan Jiang of the University of Utah for providing information on 85- and 37-GHz scattering and related figures for the strong cell in TS Gabrielle. We benefited from discussions with Dr. David Nolan of the University of Miami. We were also aided by constructive reviews from Dr. Michael Riemer and two anonymous reviewers. Data for this study came from flights by U.S. Air Force reconnaissance aircraft only 3 days after 11 September 2001. We appreciate the dedication shown by these Air Force Reserve personnel. Lixion Avila of NHC first suggested TS Gabrielle to us as a good storm to study. Gridded analyses from the ECMWF were obtained from NCAR, which is supported by the National Science Foundation (NSF). This work was supported by NSF Grants ATM0418682 and ATM0855718, and by NASA Grant NNX09AC66G.

REFERENCES

- Baker, A. K., M. D. Parker, and M. D. Eastin, 2009: Environmental ingredients for supercells and tornadoes within Hurricane Ivan. *Wea. Forecasting*, **24**, 223–244.
- Bell, M. M., and M. T. Montgomery, 2010: Sheared deep vortical convection in pre-depression Hagupit during TCS08. *Geophys. Res. Lett.*, **37**, L06802, doi:10.1029/2009GL042313.
- Biagi, C. J., K. L. Cummins, K. E. Kehoe, and E. P. Krider, 2007: National Lightning Detection Network (NLDN) performance in southern Arizona, Texas, and Oklahoma in 2003–2004. *J. Geophys. Res.*, **112**, D05208, doi:10.1029/2006JD007341.
- Black, M. L., J. F. Gamache, F. D. Marks Jr., C. E. Samsury, and H. E. Willoughby, 2002: Eastern Pacific Hurricanes Jimena of 1991 and Olivia of 1994: The effect of vertical shear on structure and intensity. *Mon. Wea. Rev.*, **130**, 2291–2312.
- Braun, S. A., and L. Wu, 2007: A numerical study of Hurricane Erin (2001). Part II: Shear and the organization of eyewall vertical motion. *Mon. Wea. Rev.*, **135**, 1179–1194.
- , M. T. Montgomery, and Z. Pu, 2006: High-resolution simulation of Hurricane Bonnie (1998). Part I: The organization of eyewall vertical motion. *J. Atmos. Sci.*, **63**, 19–42.
- Bunkers, M. J., D. R. Clabo, and J. W. Zeitler, 2009: Comments on “Structure and formation mechanism on the 24 May 2000 supercell-like storm developing in a moist environment over the Kanto Plain, Japan.” *Mon. Wea. Rev.*, **137**, 2703–2712.
- Cecil, D. J., E. J. Zipser, and S. W. Nesbitt, 2002: Reflectivity, ice scattering, and lightning characteristics of hurricane eyewalls and rainbands. Part I: Quantitative description. *Mon. Wea. Rev.*, **130**, 769–784.
- , S. J. Goodman, D. J. Boccippio, E. J. Zipser, and S. W. Nesbitt, 2005: Three years of TRMM precipitation features. Part I: Radar, radiometric, and lightning characteristics. *Mon. Wea. Rev.*, **133**, 543–566.
- Chen, S. S., J. A. Knaff, and F. D. Marks Jr., 2006: Effects of vertical wind shear and storm motion on tropical cyclone rainfall asymmetries deduced from TRMM. *Mon. Wea. Rev.*, **134**, 3190–3208.

- Corbosiero, K. L., and J. Molinari, 2002: The effects of vertical wind shear on the distribution of convection in tropical cyclones. *Mon. Wea. Rev.*, **130**, 2110–2123.
- Crum, T. D., and R. L. Alberty, 1993: The WSR-88D and the WSR-88D operational support facility. *Bull. Amer. Meteor. Soc.*, **74**, 1669–1687.
- Cummins, K. L., and M. J. Murphy, 2009: An overview of lightning locating systems: History, technique, and data uses, with an in-depth look at the U.S. NLDN. *IEEE Trans. Electromagn. Compat.*, **51**, 499–518.
- , J. A. Cramer, C. J. Biagi, E. P. Krider, J. Jeraud, M. A. Uman, and V. A. Rakov, 2006: The U.S. National Lightning Detection Network: Post-upgrade status. Preprints, *Second Conf. on Meteorological Applications of Lightning Data*, Atlanta, GA, Amer. Meteor. Soc., 6.1.
- Davies-Jones, R. P., D. Burgess, and M. Foster, 1990: Test of helicity as a tornado forecast parameter. Preprints, *16th Conf. on Severe Local Storms*, Kanaskis, Alberta, Canada, Amer. Meteor. Soc., 588–592.
- DeMaria, M., M. Mainelli, L. K. Shay, J. A. Knaff, and J. Kaplan, 2005: Further improvements to the Statistical Hurricane Intensity Prediction Scheme (SHIPS). *Wea. Forecasting*, **20**, 531–543.
- Eastin, M. D., and M. C. Link, 2009: Miniature supercells in an offshore outer rainband of Hurricane Ivan (2004). *Mon. Wea. Rev.*, **137**, 2081–2104.
- , P. G. Black, and W. M. Gray, 2002: Flight-level thermodynamic instrument wetting errors in hurricanes. Part I: Observations. *Mon. Wea. Rev.*, **130**, 825–841.
- , W. M. Gray, and P. G. Black, 2005: Buoyancy of convective vertical motions in the inner core of intense hurricanes. Part II: Case studies. *Mon. Wea. Rev.*, **133**, 209–227.
- , P. D. Reasor, D. S. Nolan, F. D. Marks Jr., and J. F. Gamache, 2006: Evolution of low-wavenumber vorticity during rapid intensification: A dual-Doppler analysis. Preprints, *27th Conf. on Hurricanes and Tropical Meteorology*, Monterey, CA, Amer. Meteor. Soc., 4B.6.
- Hanley, D., J. Molinari, and D. Keyser, 2001: A composite study of the interactions between tropical cyclones and upper-tropospheric troughs. *Mon. Wea. Rev.*, **129**, 2570–2584.
- Hart, J. A., and W. Korotky, 1991: The SHARP workstation v1.50 users guide. NOAA/National Weather Service, 30 pp. [Available from NWS Eastern Region Headquarters, 630 Johnson Ave., Bohemia, NY 11716.]
- Hendricks, E. A., M. T. Montgomery, and C. A. Davis, 2004: The role of “vortical” hot towers in the formation of Tropical Cyclone Diana (1984). *J. Atmos. Sci.*, **61**, 1209–1232.
- Heymsfield, G. M., J. B. Halverson, J. Simpson, L. Tian, and T. P. Bui, 2001: ER-2 Doppler radar investigations of the eyewall of Hurricane Bonnie during the Convection and Moisture Experiment-3. *J. Appl. Meteor.*, **40**, 1310–1330.
- , —, E. Ritchie, J. Simpson, J. Molinari, and L. Yian, 2006: Structure of the highly sheared Tropical Storm Chantal during CAMEX-4. *J. Atmos. Sci.*, **63**, 268–287.
- Houze, R. A., Jr., W.-C. Lee, and M. M. Bell, 2009: Convective contribution to the genesis of Hurricane Ophelia (2005). *Mon. Wea. Rev.*, **137**, 2778–2800.
- Kaplan, J., and M. DeMaria, 2003: Large-scale characteristics of rapidly intensifying tropical cyclones in the North Atlantic basin. *Wea. Forecasting*, **18**, 1093–1108.
- , and —, 2010: A revised tropical cyclone rapid intensification index for the Atlantic and eastern North Pacific basins. *Wea. Forecasting*, **25**, 220–241.
- Kelley, O. A., J. Stout, and J. B. Halverson, 2004: Tall precipitation cells in tropical cyclone eyewalls are associated with tropical cyclone intensification. *Geophys. Res. Lett.*, **31**, L24112, doi:10.1029/2004GL021616.
- Kim, D.-K., K. R. Knupp, and C. R. Williams, 2009: Airflow and precipitation properties within the stratiform region of Tropical Storm Gabrielle during landfall. *Mon. Wea. Rev.*, **137**, 1954–1971.
- Klazura, G. E., and D. A. Imy, 1993: A description of the initial set of analysis products available from the NEXRAD WSR-88D system. *Bull. Amer. Meteor. Soc.*, **74**, 1293–1311.
- Knupp, K. R., J. Walters, and M. Biggerstaff, 2006: Doppler profiler and radar observations of boundary layer variability during the landfall of Tropical Storm Gabrielle. *J. Atmos. Sci.*, **63**, 234–251.
- Lee, T. F., F. J. Turk, J. Hawkins, and K. Richardson, 2002: Interpretation of TRMM TMI images of tropical cyclones. *Earth Interactions*, **6**. [Available online at <http://EarthInteractions.org>.]
- Lemon, L. R., and C. A. Doswell III, 1979: Severe thunderstorm evolution and mesocyclone structure as related to tornado genesis. *Mon. Wea. Rev.*, **107**, 1184–1197.
- McCaul, E. W., Jr., 1991: Buoyancy and shear characteristics of hurricane tornado environments. *Mon. Wea. Rev.*, **119**, 1954–1978.
- , D. E. Buechler, S. J. Goodman, and M. Cammarata, 2004: Doppler radar and lightning network observations of a severe outbreak of tropical cyclone tornadoes. *Mon. Wea. Rev.*, **132**, 1747–1763.
- Mohr, K. I., and E. J. Zipser, 1996: Mesoscale convective systems defined by their 85-GHz ice scattering signature: Size and intensity comparison over tropical oceans and continents. *Mon. Wea. Rev.*, **124**, 2417–2437.
- Molinari, J., and D. Vollaro, 1989: External influences on hurricane intensity. Part I: Outflow layer eddy angular momentum fluxes. *J. Atmos. Sci.*, **46**, 1093–1105.
- , and —, 2008: Extreme helicity and intense convective towers in Hurricane Bonnie. *Mon. Wea. Rev.*, **136**, 4355–4372.
- , and —, 2010: Distribution of helicity, CAPE, and shear in tropical cyclones. *J. Atmos. Sci.*, **67**, 274–284.
- , —, and K. L. Corbosiero, 2004: Tropical cyclone formation in a sheared environment: A case study. *J. Atmos. Sci.*, **61**, 2493–2509.
- , P. Dodge, D. Vollaro, K. L. Corbosiero, and F. Marks Jr., 2006: Mesoscale aspects of the downshear reformation of a tropical cyclone. *J. Atmos. Sci.*, **63**, 341–354.
- Montgomery, M. T., M. E. Nicholls, T. A. Cram, and A. B. Saunders, 2006: A vortical hot tower route to tropical cyclogenesis. *J. Atmos. Sci.*, **63**, 355–386.
- Musgrave, K. D., C. A. Davis, and M. T. Montgomery, 2008: Numerical simulations of the formation of Hurricane Gabrielle (2001). *Mon. Wea. Rev.*, **136**, 3151–3167.
- NOAA, 2006: Federal meteorological handbook No. 11: Doppler radar meteorological observations. Part C. WSR-88D products and algorithms. Office of Federal Coordinator for Meteorology, FCM-H11C-2006, 390 pp.
- Nolan, D. S., 2007: What is the trigger for tropical cyclogenesis? *Aust. Meteor. Mag.*, **56**, 241–266.
- , Y. Moon, and D. P. Stern, 2007: Tropical cyclone intensification from asymmetric convection: Energetics and efficiency. *J. Atmos. Sci.*, **64**, 3377–3405.
- Ramsay, H. A., and C. A. Doswell, 2005: A sensitivity study of hodograph-based methods for estimating supercell motion. *Wea. Forecasting*, **20**, 954–970.

- Reasor, P. D., and M. T. Montgomery, 2001: Three-dimensional alignment and corotation of weak, TC-like vortices via linear vortex Rossby waves. *J. Atmos. Sci.*, **58**, 2306–2330.
- , —, and L. F. Bosart, 2005: Mesoscale observations of the genesis of Hurricane Dolly (1996). *J. Atmos. Sci.*, **62**, 3151–3171.
- , M. D. Eastin, and J. F. Gamache, 2009: Rapidly intensifying Hurricane Guillermo (1997). Part I: Low-wavenumber structure and evolution. *Mon. Wea. Rev.*, **137**, 603–631.
- Riemer, M., M. T. Montgomery, and M. E. Nicholls, 2010: A new paradigm for intensity modification of tropical cyclones: Thermodynamics impact of vertical wind shear on the inflow layer. *Atmos. Chem. Phys.*, **10**, 3163–3188.
- Rogers, R., 2010: Convective-scale structure and evolution during a high-resolution simulation of tropical cyclone rapid intensification. *J. Atmos. Sci.*, **67**, 44–70.
- Romps, D. M., and Z. Kuang, 2010: Do undiluted convective plumes exist in the upper tropical troposphere? *J. Atmos. Sci.*, **67**, 468–484.
- Shafer, M. A., D. R. MacGorman, and F. H. Carr, 2000: Cloud-to-ground lightning throughout the lifetime of a severe storm system in Oklahoma. *Mon. Wea. Rev.*, **128**, 1798–1816.
- Shapiro, L. J., and H. E. Willoughby, 1982: The response of balanced hurricanes to local sources of heat and momentum. *J. Atmos. Sci.*, **39**, 378–394.
- Sharp, D. W., S. M. Spratt, P. F. Blottman, and D. S. Kelly, 2002: Using high-resolution diagnostics to facilitate the short-term threat assessment of tornadoes during Tropical Storm Gabrielle (2001). Preprints, *21st Conf. on Severe Local Storms*, San Antonio, TX, Amer. Meteor. Soc., 15.3.
- Shelton, K., and J. Molinari, 2009: Life of a 6-hour hurricane. *Mon. Wea. Rev.*, **137**, 51–67.
- Simpson, J., E. Ritchie, G. J. Holland, J. Halverson, and S. Stewart, 1997: Mesoscale interactions in tropical cyclone genesis. *Mon. Wea. Rev.*, **125**, 2643–2661.
- Sippel, J. A., J. W. Nielsen-Gammon, and S. E. Allen, 2006: The multiple-vortex nature of tropical cyclogenesis. *Mon. Wea. Rev.*, **134**, 1796–1814.
- Sitkowski, M., and G. M. Barnes, 2009: Low-level thermodynamic, kinematic, and reflectivity fields of Hurricane Guillermo (1997) during rapid intensification. *Mon. Wea. Rev.*, **137**, 645–663.
- Smith, R. K., M. T. Montgomery, and N. V. Sang, 2009: Tropical cyclone spinup revisited. *Quart. J. Roy. Meteor. Soc.*, **135**, 1321–1335.
- Stewart, S. R., and S. W. Lyons, 1996: A WSR-88D radar view of Tropical Cyclone Ed. *Wea. Forecasting*, **11**, 115–135.
- Vigh, J. L., and W. H. Schubert, 2009: Rapid development of the tropical cyclone warm core. *J. Atmos. Sci.*, **66**, 3335–3350.
- Weisman, M. L., and J. B. Klemp, 1984: The structure and classification of numerically simulated convective storms in directionally varying wind shears. *Mon. Wea. Rev.*, **112**, 2479–2498.
- , and —, 1986: Characteristics of isolated convective storms. *Mesoscale Meteorology and Forecasting*, P. Ray, Ed., Amer. Meteor. Soc., 331–358.
- , and R. Rotunno, 2000: The use of vertical wind shear versus helicity in interpreting supercell dynamics. *J. Atmos. Sci.*, **57**, 1452–1472.
- Zipser, E. J., and C. Gautier, 1978: Mesoscale events within a GATE tropical depression. *Mon. Wea. Rev.*, **106**, 789–805.